RECEIVED
FEB 1 6 1999
OSTI

SAND99-0322J

PENETRATION EXPERIMENTS WITH 6061-T6511 ALUMINUM TARGETS AND SPHERICAL-NOSE STEEL PROJECTILES AT STRIKING VELOCITIES BETWEEN 0.5 AND 3.0 km/s

MICHAEL J. FORRESTAL* AND ANDREW J. PIEKUTOWSKI**
*Sandia National Laboratories, Albuquerque, NM 87185-0303, U.S.A.
**University of Dayton Research Institute, Dayton, OH 45469-0182, U.S.A.

Summary — We conducted depth of penetration experiments with 7.11-mm-diameter, 74.7-mm-long, spherical-nose, 4340 steel projectiles launched into 250-mm-diameter, 6061-T6511 aluminum targets. To show the effect of projectile strength, we used projectiles that had average Rockwell hardnesses of $R_c = 36.6$, 39.5, and 46.2. A powder gun and two-stage, light-gas guns launched the 0.023 kg projectiles at striking velocities between 0.5 and 3.0 km/s. Post-test radiographs of the targets showed three response regions as striking velocities increased: (1) the projectiles remained visibly undeformed, (2) the projectiles permanently deformed without erosion, and (3) the projectiles eroded and lost mass. To show the effect of projectile strength, we compared depth-of-penetration data as a function of striking velocity for spherical-nose rods with three Rockwell hardnesses at striking velocities ranging from 0.5 to 3.0 km/s. To show the effect of nose shape, we compared penetration data for the spherical-nose projectiles with previously published data for ogive-nose projectiles.

Keywords: penetration, aluminum targets, spherical-nose steel projectiles.

DISCLAIMER

DISCLAIMER

Introduction

Most studies of long-rod projectiles launched at targets to large striking velocities have focused on tungsten projectiles and steel or contained ceramic targets. Silsby [1] conducted experiments with tungsten alloy, long rods and armor steel targets at striking velocities between 1.3 and 4.5 km/s. For those experiments, depth of penetration increased monotonically and eventually reached a plateau as striking velocity increased. Anderson *et al.* [2] present data from Silsby [1] and five other studies and show a small data scatter from all six studies for tungsten rod projectiles with length-to-diameter ratios of 20. This same relationship between penetration depth versus striking velocity was reported recently for contained ceramic targets by Orphal *et al.* [3]. For these very resistive steel and contained ceramic targets, the projectile deforms at impact and erodes during the penetration process.

By contrast, Forrestal *et al.* [4] present depth of penetration data for 6061-T651 aluminum targets and C-300 maraging steel [5], spherical-nose rods that showed the projectiles remained visibly undeformed for striking velocities to 1.16 km/s. Penetration depth increased with striking velocities to 1.16 km/s, but for larger striking velocities the projectile shanks fractured into several segments in the penetration channel.

In this study, we used vacuum-arc remelted (VAR) 4340 steel projectiles with average Rockwell hardnesses of R_c = 36.6, 39.5, and 46.2 [6] and 6061-T6511 aluminum targets. We changed from maraging steel projectiles [4] to 4340 steel projectiles, avoided shank fractures, and conducted experiments with striking velocities between 0.5 and 3.0 km/s. Post-test radiographs of the targets showed three response regions as striking velocity increased: (1) the projectiles remained visibly undeformed, (2) the projectiles permanently deformed without erosion, and (3) the projectiles eroded and lost mass. To show the effect of projectile strength, we compared depth-of-penetration data from spherical-nose projectiles with three hardnesses. In addition, we compared depth-of-penetration data for the spherical-nose projectiles with data for ogive-nose projectiles [7].

Experiments

We conducted depth of penetration experiments with the spherical-nose, steel projectile dimensioned in Fig. 1 and 250-mm-diameter 6061-T6511 aluminum targets. Tables 1, 2, and 3 summarize results from 31 experiments for striking velocities between 496 and 3075 m/s. To avoid projectile shank fracture and to show the effect of projectile hardness, we made the projectiles from vacuum-arc-remelted (VAR) 4340 steel. The average Rockwell hardnesses for the data sets given in Tables 1, 2, and 3 are R_c = 36.6, 39.5, and 46.2, respectively. The relationships between heat treatment, hardness, and yield strength for 4340 steel are given in [6]. In addition, we obtained uniaxial stress-strain data for the target and projectile materials at strain rates from 10^{-3} to $10^6 s^{-1}$. These data and constitutive models are presented in [8, 9].

A 20-mm powder gun launched the projectiles for striking velocities less than 1337 m/s. For larger striking velocities, the projectiles were launched with a 50/20 mm or a 75/30-mm, two-stage, light-gas gun [10]. In Tables 1, 2, and 3, shot numbers that begin with one, four, and eight correspond to the 20-mm powder gun, the 50/20-mm light-gas gun, and the 75/30-mm light-gas gun, respectively. With these three launchers, we were able to obtain the range of striking velocities listed in Tables 1, 2, and 3. Projectile striking velocities were measured with an accuracy of better than one-half percent with laserphotodetectors stationed at four locations along the flight path. Pitch and yaw were measured from radiographs obtained from an orthogonal pair of flash x-rays positioned immediately in front of the target. Penetration depth and final projectile shape were determined from post-test radiographs of 38-mm-thick slices of the targets. The target slices were cut with special care to ensure the planes of maximum inclination of the projectiles were coincident with the planes of the slices.

Figures 2 and 3 show selected radiographs of the post-test targets from the series of experiments summarized in Table 2. Shot number 1-0405 with $V_s = 781$ m/s and shot number 1-0402 with $V_s = 932$ m/s in Fig. 2 show the projectiles have slight bulges near the spherical nose and some shank bending. Shot number 1-0404 with $V_s = 1037$ m/s in Fig. 2 shows a large bulge over about one-half of the deformed projectile length and a kinked projectile that deviates severely from the shot line. Data in Table 2 show an increase in penetration depth as striking velocity increases until shot number 1-0403 with $V_s = 967$ m/s and a dramatic change in penetration depth for shot number 1-0404 with $V_s = 1037$ m/s (see Fig. 2). In addition, the last column of Table 2 records the change in length of the deformed projectiles, ΔL. The data in Table 2 and the radiographs in Fig. 2 display clearly that the projectile permanent plastic deformation increases with striking velocity until the projectile develops a large bulge and a kink. These observations will be further explained in the next section when we present depth of penetration versus striking velocity data.

Figure 3 shows post-test radiographs of the targets for projectiles that eroded and lost mass. In Fig. 3, we present results from shot number 1-0406 with V_s = 1193 m/s, shot number 4-1826 with V_s = 1802 m/s, and shot number 8-0105 with V_s = 3075 m/s. These three radiographs show typical eroding rod behavior.

In summary, the data in Table 2 and radiographs in Figs. 2 and 3 show the projectile final conditions as striking velocity increases from 496 m/s to 3075 m/s. For the lower striking velocities, the projectiles are visibly undeformed. As striking velocity increases, projectile plastic deformation increases until the projectile develops a large bulge and a kink (see Fig. 2). Finally, for large enough striking velocity, the projectiles erode and lose mass (see Fig. 3). Again, these data will be further discussed in the next section when we present plots of depth of penetration versus striking velocity.

Ballistic Performance

In this section, we show plots of penetration depth versus striking velocity for the data in Tables 1, 2, and 3. As previously discussed, post-test radiographs of the targets showed three response regions as striking velocities increased: (1) the projectiles remained visibly undeformed, (2) the projectiles permanently deformed without erosion, and (3) the projectiles eroded and lost mass. Figure 4 shows depth of penetration versus striking velocity data given in Tables 1, 2, and 3 for the first two response regions. In addition, Fig. 4 contains three data points from previously conducted experiments that used maraging C-300 steel, spherical-nose rods [4], and a prediction from our rigid projectile model [9]. While the maraging C-300 steel projectiles remained visibly undeformed [4], all the 4340 steel projectiles used in this study had some permanent deformation. Tables 1, 2, and 3 record the post-test change of length, ΔL, of the projectiles that did not erode and lose mass. Figure 4 shows that all the 4340 steel data lie on or below the prediction for a rigid projectile. For shots 1-0413, 1-0416, and 1-0409, the post-test changes in projectile lengths were 0.8, 1.2, and 0.5 mm, which are very small, and these three data points lie on or very close to the rigid projectile model prediction. However, as the changes of projectile lengths increase, the data lie further below the rigid projectile model prediction. The data plotted in Fig. 4

from Tables 1, 2, and 3 for the average Rockwell hardnesses of 36.6, 39.5, and 46.2 also show the effect of hardness on ballistic performance.

In Fig. 5, we plot all of the data given in Tables 1, 2, and 3 for the final projectile shapes that range from visibly undeformed to highly eroded. The dashed lines in Fig. 5 are a second order polynomial fit to the data. Again, the post-test radiographs in Fig. 2 and penetration depth data in Fig. 5 show an increase in depth of penetration as striking velocity increases until the projectile develops a large bulge and a kink. As the striking velocity gets larger, the projectiles erode and lose mass (see Fig. 3). For the data in Table 2, the projectile has some bulging and slight bending for shot number 1-0403 with V_s = 967 m/s, the projectile has a large bulge and kinks for shot number 1-0404 with V_s = 1037 m/s (see Fig. 2), and the projectile has eroded and lost mass for shot number 1-0406 with V_s = 1193 m/s (see Fig. 3). Thus, there is a transition response region between V_s = 967 m/s and V_s = 1037 m/s that separates the plastically deformed and eroded projectiles. Figure 5 shows the different final projectile response regions and the effect of hardness on ballistic performance.

In a recent study [7], we performed a similar set of experiments with 7.11-mm-diameter, 71.12-mm-long, ogive-nose, steel projectiles and 254-mm-diameter, 6061-T6511 aluminum targets. The projectiles were made with VAR 4340 steel, had an average Rockwell hardness of 38.4, had a 3.0 caliber-radiushead (CRH) nose-shape, and a mass of 0.021 kg. Other than a different nose-shape, the geometries and materials used in [7] and in this study were nearly the same. As previously discussed, all the 4340 steel, spherical-nose projectiles used in this study permanently deformed. In particular, the spherical-nose projectiles hardened to an average of R_c 39.5, showed permanent nose and shank deformations without erosion for $496 < V_s < 967$ m/s, and an eroded behavior for $1193 < V_s < 3075$ m/s. By contrast, the 3.0 CRH, R_c 38.4 projectiles [7] showed no visible nose deformations for $569 < V_s < 1396$ m/s. For striking velocities below 1237 m/s, the 3.0 CRH projectiles remained visibly undeformed and the penetration channels were straight; however, for $V_s = 1365$ and 1396 m/s, the penetration channels were curved, the shanks were bent, and the noses remained undeformed. Thus, maximum depth of penetration for the 4340 R_c 39.5 steel, spherical-nose projectiles is limited by plastic deformation whereas maximum penetration depth for the 4340 R_c 38.4 steel, 3.0 CRH ogive-nose projectiles is limited by shank bending that causes the projectile to deviate from the shot line.

In Fig. 6, we compare normalized penetration depth versus striking velocity for spherical-nose and ogive-nose projectiles. As mentioned, these projectiles have slightly different masses and a different nose shape. From [11], the projectile mass for a spherical-nose or ogive-nose projectile is given by

$$m = \pi a^2 \rho \left[L + ka\right] \tag{1}$$

where a is the shank radius, L is the shank length, ρ is the projectile density, and k depends on the nose shape [11]. For the spherical-nose projectile, $k = 0.667$, and for the 3.0 CRH ogive-nose projectile, $k = 1.813$. Since the a and ρ are the same for both projectiles, we plotted the normalized penetration depth $P/(L + ka)$ in Fig. 6. The spherical-nose projectile dimensions are given in Fig. 1 and $(L + ka) = 73.5$ mm. The ogive-nose projectile [7] has shank length $L = 59.3$ mm and $(L + ka) = 65.8$ mm.

Figure 6 shows that our analytical model for rigid projectiles [7, 9] is in good agreement with the ogive-nose data and that the spherical-nose data lie on or below the prediction. As previously mentioned, the ogive-nose projectiles remained visibly undeformed, whereas the spherical-nose projectiles experienced increasing plastic deformation as striking velocity increased. We used polynomial data fits of order two through the data in the regions where the projectiles erode. Figure 6 shows clearly the superior performance of the ogive-nose projectiles.

Conclusions

We present depth of penetration data for 4340 steel, spherical-nose projectiles and 6061-T6511 targets. A powder gun and two-stage, light-gas guns launched 0.023 kg projectiles to striking velocities between 0.5 and 3.0 km/s. Post-test radiographs of the targets identified three response regions as striking velocity increased: (1) the projectiles remained visibly undeformed, (2) the projectiles permanently deformed without erosion, and (3) the projectiles eroded and lost mass. Data from projectiles with average hardnesses of R_c = 36.6, 39.5, and 46.2 showed the effect of projectile strength on ballistic performance. To show the effect of nose shape, we compared penetration data for the spherical-nose projectiles and previously published data for ogive-nose projectiles.

Acknowledgment—This work was supported by the United States Department of Energy and the Joint DoD/DOE Munitions Technology Development Program. Sandia is a multiprogram laboratory operated by Sandia Corporation, a Lockheed Martin Company, for the United States Department of Energy under Contract DE-AC04-94AL85000. The authors also thank Dr. T. L. Warren for many helpful suggestions.

References

[1] G. F. Silsby. Penetration of semi-infinite steel targets by tungsten rods at 1.3 to 4.5 km/s. *Proc. 8th Int. Symp. Ballistics*, TB/31–35, Orlando, Florida. (1984).

[2] C. E. Anderson, S. A. Mullin, A. J. Piekutowski, N. W. Blaylock, and K. L. Poormon. Scale model experiments with ceramic laminate targets. *International Journal of Impact Engineering* **18**, 1–22. (1996).

[3] D. L. Orphal, R. R. Franzen, A. J. Piekutowski, and M. J. Forrestal. Penetration of confined aluminum nitride targets by tungsten long rods at 1.5–4.5 km/s. *International Journal of Impact Engineering* **18**, 355–386. (1996).

[4] M. J. Forrestal, K. Okajima, and V. K. Luk. Penetration of 6061-T651 aluminum targets with rigid long rods. *ASME Journal of Applied Mechanics* **55**, 755–760. (1988).

[5] INCO Data Bulletin. 18% Nickel Maraging Steels, The International Nickel Company, Inc., 67 Wall Street, New York, NY, 10005. (1964).

[6] W. F. Brown, H. Mindlin, and C. Y. Ho. *Aerospace Structural Metals Handbook, Vol. 1*, Code 1206, 1–45. (1996).

[7] A. J. Piekutowski, M. J. Forrestal, K. L. Poormon, and T. L. Warren. Penetration of 6061-T6511 aluminum targets by ogive-nose steel projectiles with striking velocities between 0.5 and 3.0 km/s. *International Journal of Impact Engineering* (in press).

[8] T. L. Warren and M. R. Tabbara. Simulations of the penetration of 6061-T651 aluminum targets by spherical-nosed VAR 4340 steel projectiles. (submitted).

[9] T. L. Warren and M. J. Forrestal. Effects of strain hardening and strain-rate sensitivity on the penetration of aluminum targets with spherical-nosed rods. *International Journal of Solids and Structures* **35**, 3737–3753. (1998).

[10] A. J. Stilp and V. Hohler. Experimental methods for terminal ballistics and impact physics. *High Velocity Impact Dynamics*, Chapter 8, J. A. Zukas (Ed.), John Wiley and Sons, Inc., New York, NY. (1990).

[11] M. J. Forrestal, V. K. Luk, Z. Rosenberg, and N. S. Brar. Penetration of 7075-T651 aluminum targets with ogive-nose rods. *International Journal of Solids and Structures* **29**, 1729–1736. (1992).

Table 1. Data summary for the projectiles with average hardness, R_c = 36.6. For pitch and yaw: D = down, U = up, R = right, L = left.

Shot number	Target length (mm)	Projectile mass m(g)	Projectile hardness R_c	Striking velocity V_s (m/s)	Pitch, yaw (degrees)	Penetration depth P(mm)	Projectile length change ΔL(mm)
1-0394	216	22.83	36.8	720	1.0 D, 0	67.8	3.3
1-0398	152	22.83	36.7	806	1.75 D, 0	74.7	6.6
1-0399	178	22.83	36.4	892	0.75 U, 0.5 L	84.1	9.4
1-0395	216	22.80	36.4	1042	0, 0	41.6	
1-0396	241	22.83	36.7	1216	0.5 U, 0.25 R	50.7	
8-0106	241	22.83	36.4	2479	1.75 D, 0.25 L	137.9	

Table 2. Data summary for the projectiles with average hardness, R_c = 39.5. For pitch and yaw: D = down, U = up, R = right, L = left.

Shot number	Target length (mm)	Projectile mass m(g)	Projectile hardness R_c	Striking velocity V_s (m/s)	Pitch, yaw (degrees)	Penetration depth P(mm)	Projectile length change ΔL(mm)
1-0413	114	22.86	39.3	496	0, 0.25 R	37.6	0.8
1-0416	121	22.83	38.6	572	1.25 U, 0	48.1	1.2
1-0405	124	22.84	39.7	781	1.5 D, 2.5 R	72.7	4.6
1-0417	152	22.84	40.0	821	0.75 D, 1.5 L	84.3	4.0
1-0400	178	22.83	39.3	841	0, 0	91.4	2.5
1-0402	178	22.84	39.3	932	0.5 D, 0.5 L	96.5	6.6
1-0403	178	22.84	39.7	967	0, 0.25 L	94.4	10.2
1-0404	178	22.84	39.6	1037	0, 0.5 L	64.6	
1-0406	175	22.85	39.4	1193	0.25 U, 1.0 L	50.7	
1-0397	297	22.83	39.4	1337	0.5 D, 0.25 R	61.8	
4-1827	178	22.84	39.7	1515	0.75 D, 1.25 L	76.0	
4-1826	190	22.85	39.7	1802	2.5 D, 1.0 R	94.3	
4-1825	216	22.83	39.7	2052	0.25 D, 1.0 R	113.9	
8-0107	241	22.85	39.6	2204	1.5 D, 0.9 L	124.6	
8-0116	241	22.84	40.2	2777	2.75 D, 3.0 L	147.0	
8-0105	241	22.84	39.0	3075	3.0 D, 4.25 L	151.0	

Table 3. **Data summary for the projectiles with average hardness, R_c = 46.2. For pitch and yaw: D = down, U = up, R = right, L = left.**

Shot number	Target length (mm)	Projectile mass m(g)	Projectile hardness R_c	Striking velocity V_s (m/s)	Pitch, yaw (degrees)	Penetration depth P(mm)	Projectile length change ΔL(mm)
1-0409	184	22.84	45.6	909	0.5 U, 0	109.6	0.5
1-0407	197	22.81	45.8	1086	0, 0	126.3	6.4
1-0411	203	22.81	46.1	1174	0.5 U, 0.5 L	67.5	
1-0408	208	22.82	45.9	1174	0, 0.5 R	66.5	
1-0410	156	22.84	45.6	1284	0.5 U, 0	78.8	
4-1828	151	22.82	46.4	1411	1.25 D, 0.75 R	106.1	
4-1838	254	22.77	46.8	1813	1.75 U, 0.75 L	120.0	
4-1834	214	22.83	46.6	2255	4.0 D, 5.0 R	137.4	
8-0115	240	22.70	46.7	2787	3.25 D, 4.75 L	159.0	

List of Figure Captions

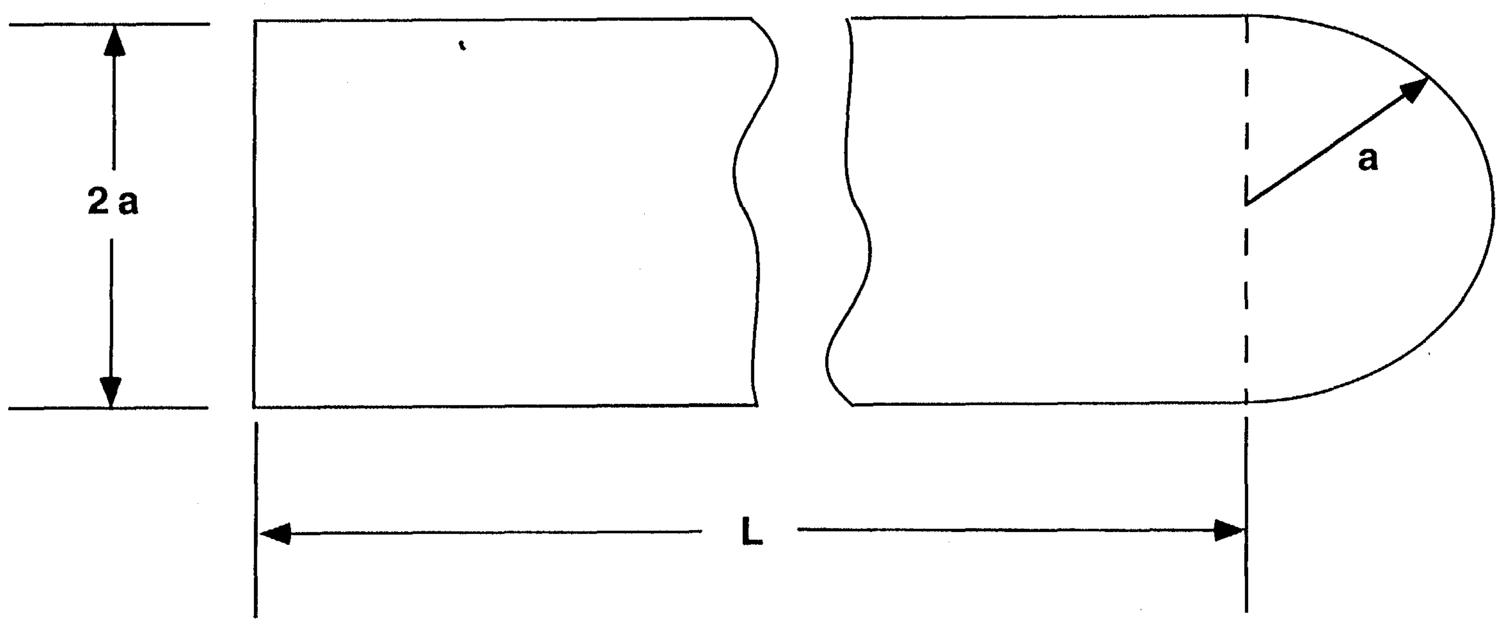

2 a
a
L

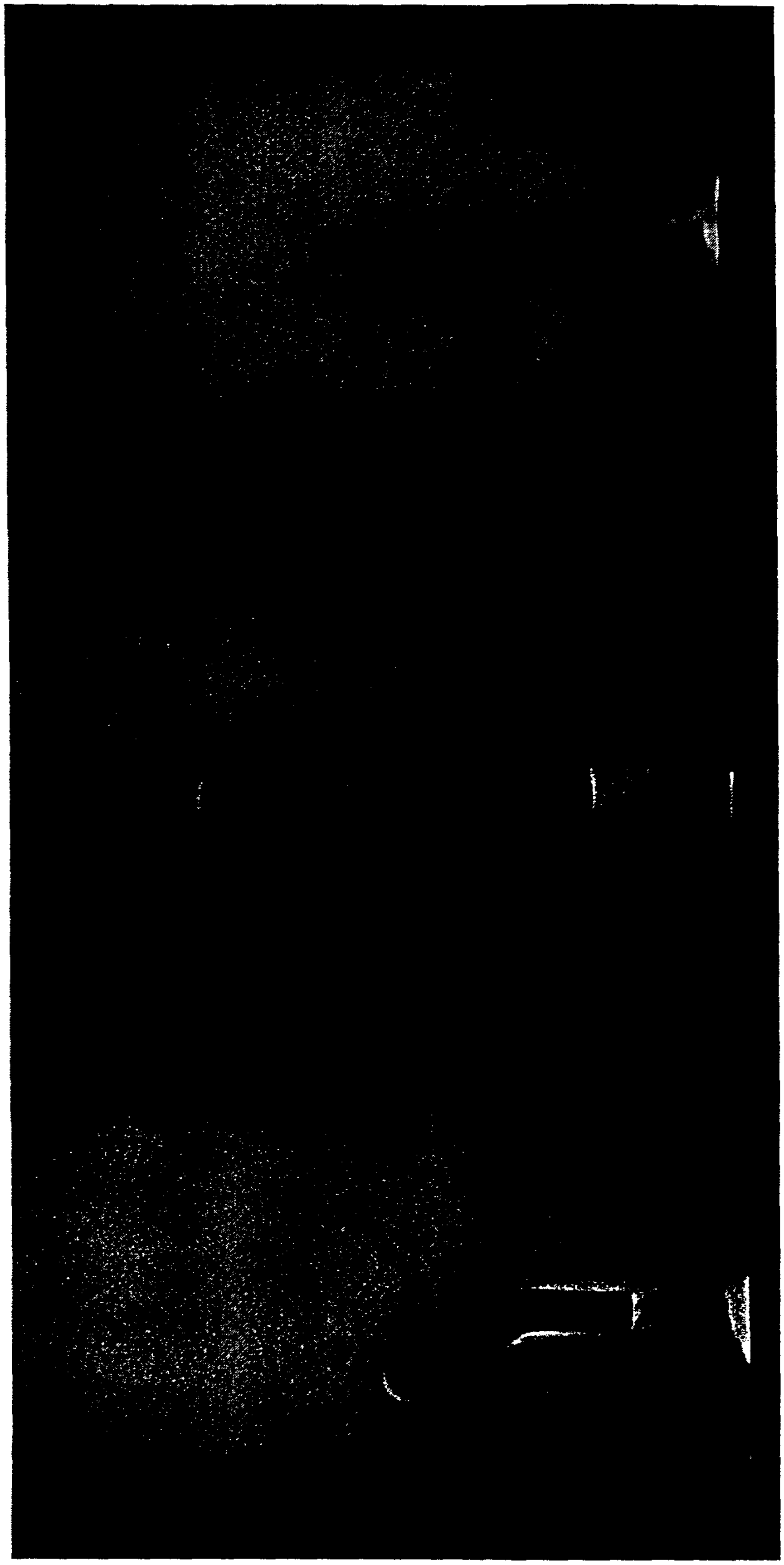

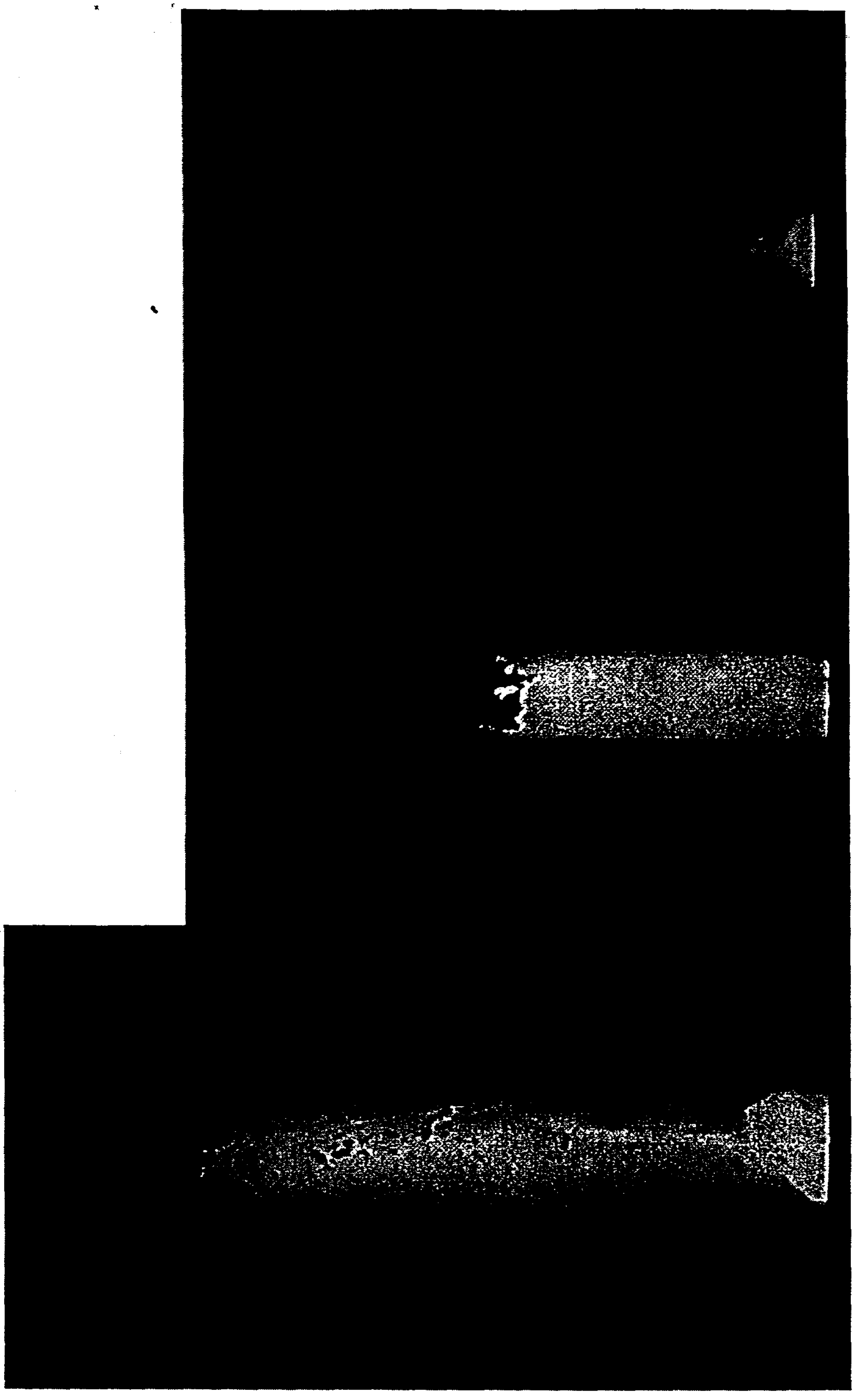

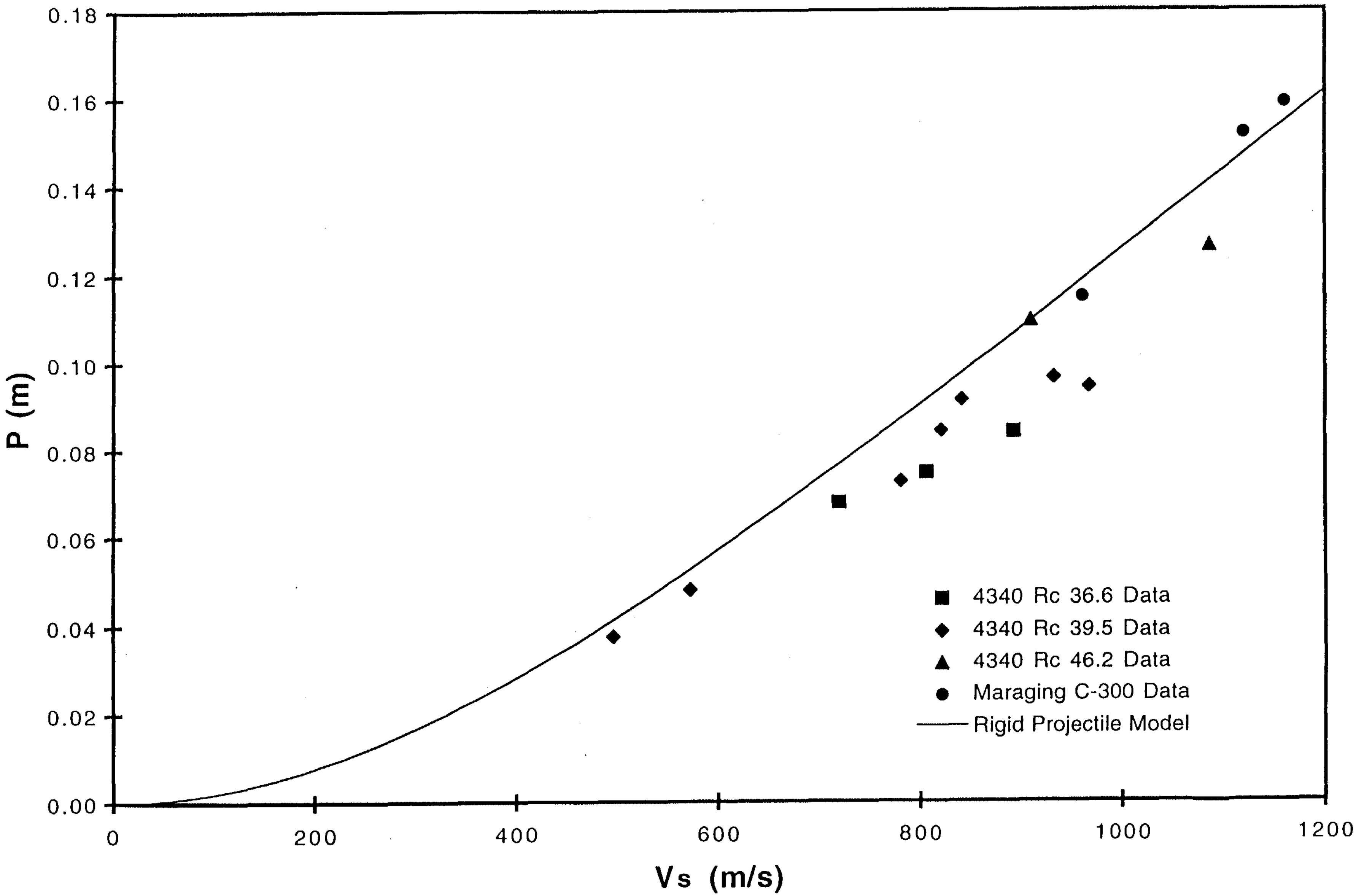

P (m)
0.18
0.16
0.14
0.12
0.10
0.08
0.06
0.04
0.02
0.00
0
200
400
600
800
1000
1200
Vs (m/s)
4340 Rc 36.6 Data
4340 Rc 39.5 Data
4340 Rc 46.2 Data
Maraging C-300 Data
Rigid Projectile Model

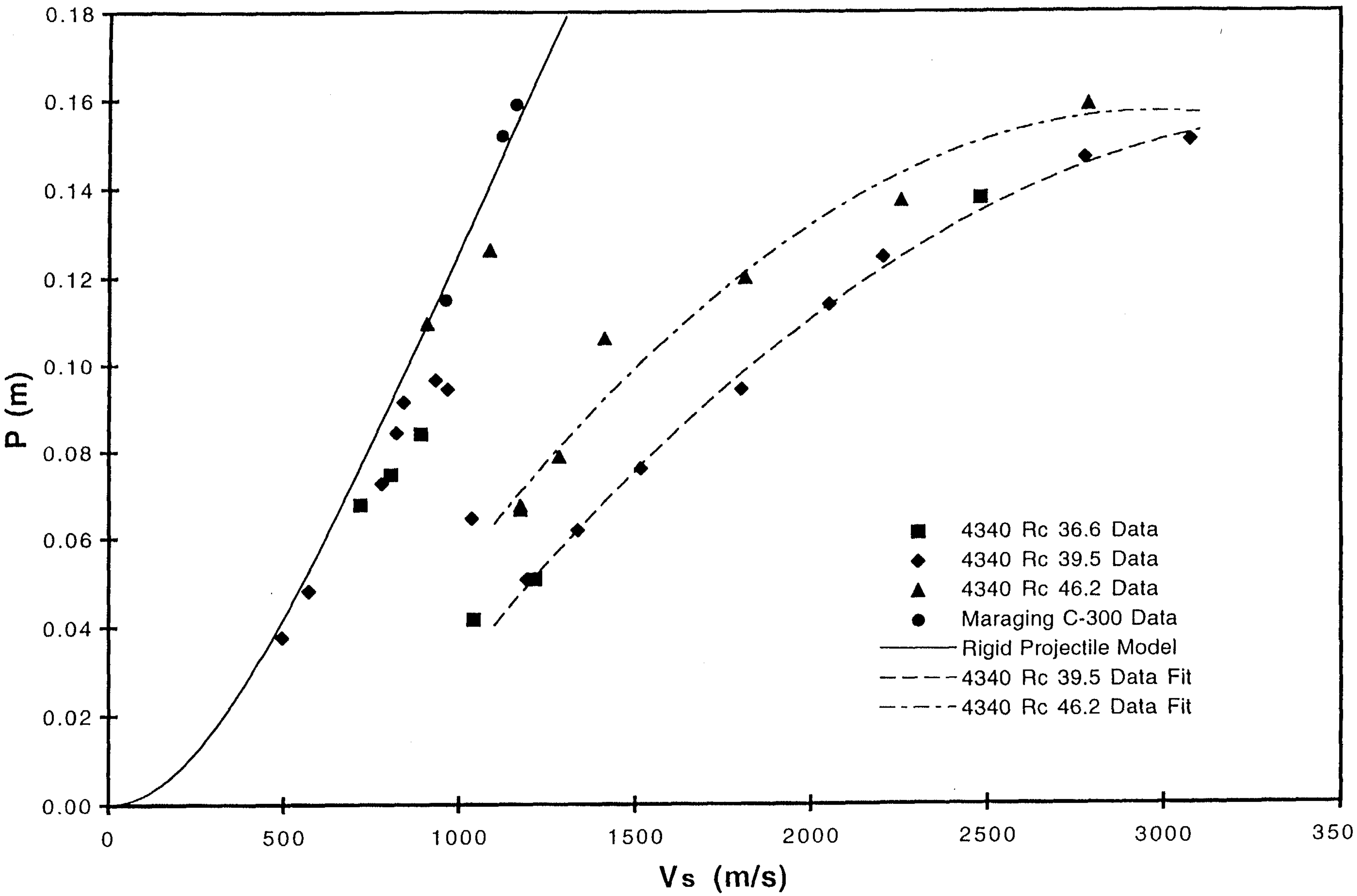

0.18
0.16
0.14
0.12
0.10
0.08
0.06
0.04
0.02
0.00
P (m)
0
500
1000
1500
2000
2500
3000
3500
Vs (m/s)
4340 Rc 36.6 Data
4340 Rc 39.5 Data
4340 Rc 46.2 Data
Maraging C-300 Data
Rigid Projectile Model
4340 Rc 39.5 Data Fit
4340 Rc 46.2 Data Fit

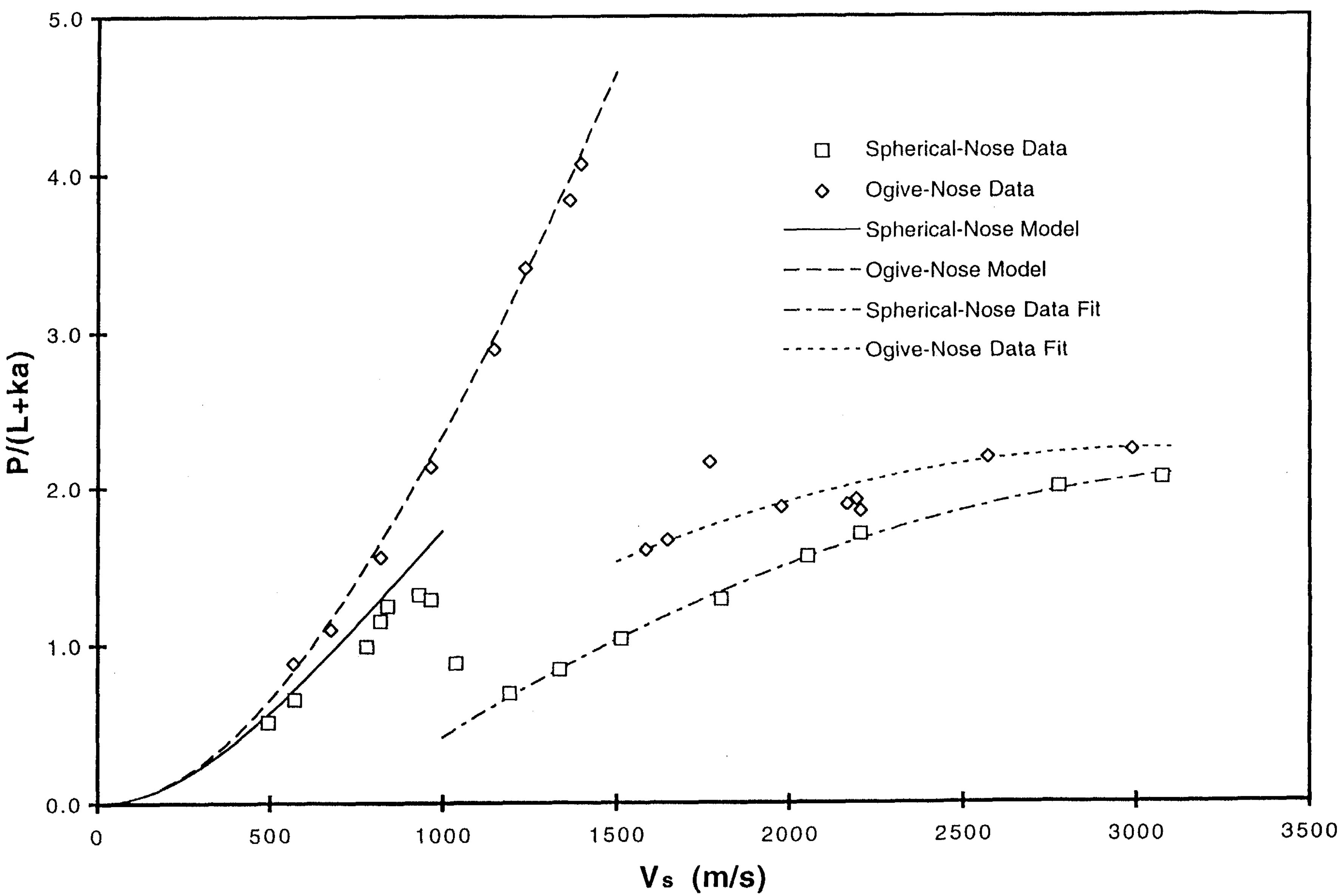
Spherical-Nose Data
Ogive-Nose Data
Spherical-Nose Model
Ogive-Nose Model
Spherical-Nose Data Fit
Ogive-Nose Data Fit
P/(L+ka)
Vs (m/s)
0.0
1.0
2.0
3.0
4.0
5.0
0
500
1000
1500
2000
2500
3000
3500